MultiScience - XXXIII. microCAD International Multidisciplinary Scientific Conference
University of Miskolc, 23-24 May, 2019, ISBN 978-963-358-177-3

HIGH-ORDER NUMERICAL METHODS FOR RELATIVISTIC HYDRODYNAMICS − PART I: THEORY AND METHODOLOGY

Jamie F. Townsend[1], László Könözsy[2], Karl W. Jenkins[3]
[1]Ph.D. Student, *Centre for Computational Engineering Sciences, Cranfield University, Cranfield, Bedfordshire, MK43 0AL, United Kingdom*
[2]Senior Lecturer, *Centre for Computational Engineering Sciences, Cranfield University, Cranfield, Bedfordshire, MK43 0AL, United Kingdom*
[3]Associate Professor, *Centre for Computational Engineering Sciences, Cranfield University, Cranfield, Bedfordshire, MK43 0AL, United Kingdom*

ABSTRACT

A recently developed numerical solver for relativistic hydrodynamics, eCOS, is presented. The governing equations and subsequent solution methodology are described followed by a demonstration of its predictive capability. High-fidelity numerical solutions are achieved regarding the solution of problems involving in one- and two-dimensional test cases containing strong shock-waves and complex flow features. eCOS is shown to be competitive with other solvers of this nature found in the current literature. All validation test cases provide confidence in its ability, both qualitatively and quantitatively, such that the solver is commissioned to study problems that do not have a known solution and thus require a numerical approximation.

1. INTRODUCTION

Research into numerical methods for relativistic hydrodynamics (RHD) has witnessed a becoming trend throughout recent decades (see [1, 2] for comprehensive reviews). Relativity is a necessary descriptor in many astrophysical and high-energy phenomenon; including its effects within a fluid system are pertinent to the study of various applications. Heavy-ion collisions offer one source of motivation as the matter created in the experiments at facilities such as CERN and the Relativistic Heavy Ion Collider (RHIC) use the hydrodynamic model to interpret their experimental findings [3]. Due to the near light-speed velocities the particles are accelerated to, relativistic effects must be considered in any numerical solutions. Relativistic hydrodynamics can play a role in the computational study of inertial confinement fusion (ICF) [4] where a nuclear fusion reaction is attempted by heating and compressing a hydrogen fuel target by means of high-energy lasers. Astrophysical applications include: relativistic jets, gamma-ray bursts and pulsar wind nebulae; see [2] for an excellent summary.

In all of the aforementioned scenarios the ability to numerically solve the RHD equations is crucial. This has been achieved by many authors in the context of Godunov-type methods and high-orders of accuracy have been achieved e.g. in [5].

In this report a new code, eCOS, for numerically solving the relativistic hydrodynamics equations is presented using state-of-the-art high-order numerical methods. A test suite of one- and two-dimensional problems is presented in order to demonstrate the

DOI: 10.26649/musci.2019.054

predictive capability of the solver alongside the governing equations and solution methodology. Throughout this report, natural units are used such that speed of light is

set equal to unity, $c = 1$.

2. MATHEMATICAL FORMULATION

The coupling of space and time is a fundamental principle built into relativity. To encompass this a fluid four-velocity is defined such that the velocity of the fluid can be described from different inertial frames of reference. The fluid four-velocity is expressed as $u^\mu = W(1, u^i)$ where the Greek indices are $\mu, \nu = 0 \ldots 4$ and the Roman, $i, j = 1 \ldots 3$ are used to describe the spatial component. When operating under the assumption of a flat spacetime, i.e. general relativistic effects are not accounted for, the Minkowski metric is used. This is given the form $g^{\mu\nu} = \mathrm{diag}(-1,1,1,1)$. A stress-energy tensor for a perfect fluid is given by

$$T^{\mu\nu} = \rho h u^\mu u^\nu + p g^{\mu\nu}, \tag{1}$$

where p is the fluid pressure and h is the specific enthalpy which is defined for an ideal-fluid as $h = 1 + \epsilon + p/\rho$, with ϵ denoting the specific internal energy of the fluid. The equations of motion for RHD are found by the following conservation laws

$$(\rho u^\mu)_{;\mu} = 0, \tag{2}$$
$$T^{\mu\upsilon}{}_{;\upsilon} = 0, \tag{3}$$

where ; μ represents the covariant derivative with respect to the coordinate x^μ. The equations of RHD can be written as a system of conservation laws applicable to modern-day High-Resolution Shock-Capturing (HRSC) methods. These equations lend themselves nicely to numerical integration, in particular when the (3+1) "Valencia" formulation is adopted [6]. The governing equations of RHD are expressed as

$$\frac{\partial \boldsymbol{U}}{\partial t} + \frac{\partial \boldsymbol{F}^x(\boldsymbol{U})}{\partial x} + \frac{\partial \boldsymbol{F}^y(\boldsymbol{U})}{\partial y} = 0, \tag{4}$$

whereby the conserved variables $\boldsymbol{U}$ that are evolved in time are given by

$$\boldsymbol{U} = \begin{pmatrix} D \\ \boldsymbol{S}^{(x)} \\ \boldsymbol{S}^{(y)} \\ \tau \end{pmatrix} = \begin{pmatrix} \rho W \\ \rho h W^2 u \\ \rho h W^2 v \\ \rho h W^2 - p - D \end{pmatrix}. \tag{5}$$

Expressions for the mass density D, the x- and y-momentum $\boldsymbol{S}^{(x,y)}$ and the total energy τ are comprised of the primitive variables: rest-mass density ρ, Lorentz factor W, pressure p, x- and y-velocities u and v and the specific enthalpy h. The Lorentz factor is given by $W = 1/\sqrt{1 - \boldsymbol{u}^2}$. The corresponding numerical fluxes $\boldsymbol{F}^{x,y}$ are given by

$$\boldsymbol{F}^x = \begin{pmatrix} D v^x \\ \boldsymbol{S}^x v^x + p \\ \boldsymbol{S}^y v^x \\ \boldsymbol{S}^x - D v^x \end{pmatrix}, \quad \boldsymbol{F}^y = \begin{pmatrix} D v^y \\ \boldsymbol{S}^x v^y \\ \boldsymbol{S}^y v^y + p \\ \boldsymbol{S}^y - D v^y \end{pmatrix}. \tag{6}$$

Finally, the system is closed via an equation of state. In this work an ideal Γ-law gas is assumed, $p = (\Gamma - 1)\rho\varepsilon$ where Γ is the constant adiabatic index of the fluid. The speed of sound is found by $c_s^2 = \Gamma p/\rho h$.

The equations presented form a hyperbolic system of equations [7]. This mathematical structure means the Jacobian of the fluxes have real and distinct eigenvalues with a complete set of eigenvectors. This entails that solution information propagates at finite velocities, provided from the Jacobian eigenvalues, and are related to the speeds of flow disturbances, i.e. entropy and sound waves. This enables the application of HRSC methods to be easily applied which is largely based on knowledge gained from solving the Euler equations in Newtonian physics. From the spectral decomposition of Eq. (4), the eigenvalues found in the x-direction for a two-dimensional system are

$$\lambda_0 = v_x \text{ (double)}, \tag{7a}$$

$$\lambda_{\pm} = \frac{1}{1-\boldsymbol{v}^2 c_s^2}\left\{v_x(1-c_s^2) \pm c_s\sqrt{(1-\boldsymbol{v}^2)[1-v_x v_x - (\boldsymbol{v}^2 - v_x v_x)c_s^2]}\right\}. \tag{7b}$$

The eigenvalues are required for computing the time-step in Eq. (13) and obtaining the left and right wave speeds necessary for the solution of the local Riemann problem in Eq. (8). Eigenvalues corresponding to the y-direction are easily found by symmetry considerations.

3. NUMERICAL METHODS

The numerical methods manifest within eCOS comply with the standard HRSC framework in conjunction with a Godunov-type philosophy. eCOS is a finite volume (FV) solver based on a cell-centre discretisation.

At the heart of HRSC Godunov-type schemes is the numerical solution to the local Riemann problem. This solution enables the calculation of the intercell numerical flux. Several means to achieve this using a Riemann solver are available using approximate, linearised and exact Riemann solvers, details of which in the context of RHD and RMHD can be found in [2].

In this study only the HLL Riemann solver is considered as it is a popular choice within many RHD codes due to its simplicity and accuracy, [8]. The HLL Riemann solver assumes that after the decay of the initial discontinuity, two waves propagate in different directions with speeds S_L and S_R separated by one constant state. The numerical flux is then calculated from

$$\boldsymbol{F}^{HLL} = \begin{cases} \boldsymbol{F}_L & \text{if} \quad 0 < S_L \\ \boldsymbol{F}_* & \text{if} \quad S_L < 0 < S_R, \\ \boldsymbol{F}_R & \text{if} \quad 0 > S_R \end{cases} \tag{8}$$

where the fluxes $\boldsymbol{F}_L$ and $\boldsymbol{F}_R$ are computed from (6) and the flux in the intermediate state $\boldsymbol{F}_*$ is computed via

$$\boldsymbol{F}_* := \frac{S_R\boldsymbol{F}_L - S_L\boldsymbol{F}_R + S_L S_R(\boldsymbol{U}_R - \boldsymbol{U}_L)}{S_R - S_L}. \tag{9}$$

The wave speeds S_L and S_R are computed from the positive and negative eigenvalues and applied to the following relations

$$S_L := \min(0, \lambda_-(\boldsymbol{U}_L), \lambda_-(\boldsymbol{U}_L)), \tag{10}$$
$$S_R := \min(0, \lambda_+(\boldsymbol{U}_L), \lambda_+(\boldsymbol{U}_L)), \tag{11}$$

where λ_- and λ_+ are given by Eq. (7).

To obtain the initial left and right states for the local Riemann the WENO reconstruction method is used. This process performs the spatial reconstruction in terms of the primitive variables and not the conserved ones, as is commonly done in Newtonian hydrodynamics. This avoids excessive oscillations and therefore achieves improved accuracy and numerical stability [9].

The WENO method uses a series of polynomial stencils to interpolate the primitive variables around a given point. A weight of these stencils is then computed to determine if a discontinuity lies amongst them. For a 5th-order reconstruction three 3rd-order stencils will be used. The reconstruction polynomial will then be 5th-order accurate in smooth regions but if a discontinuity is found then weighting will reduce the order automatically so as not to include the stencil containing the discontinuity in the final reconstruction. Therefore, a 5th-order reconstruction is 5th-order accurate in smooth regions but 3rd-order accurate in regions surrounding a discontinuity.

To advance the solution in time using the conserved variables a 3rd-order Total Variation Diminishing (TVD) Runge–Kutta (RK3) method is used. The RK3 method is given by

$$\begin{aligned} \boldsymbol{U}^{(1)} &= \boldsymbol{U}^n + \Delta t Q(\boldsymbol{U}^n), \\ \boldsymbol{U}^{(2)} &= \tfrac{1}{4}\left[3\boldsymbol{U}^n + \boldsymbol{U}^{(1)} + \Delta t Q(\boldsymbol{U}^{(1)})\right], \\ \boldsymbol{U}^{n+1} &= \tfrac{1}{3}\boldsymbol{U}^n + \tfrac{2}{3}\boldsymbol{U}^{(2)} + \tfrac{2}{3}\Delta t Q(\boldsymbol{U}^{(2)}), \end{aligned} \tag{12}$$

where Q corresponds to the intercell numerical flux value obtained form (8). For the RK3 method to remain TVD an appropriate time-step, Δt, must be supplied. For a two-dimensional ($Dim = 2$) system this is given as

$$\Delta t = \frac{\mathrm{CFL}}{Dim} \min\left(\frac{\Delta x}{|\lambda_x|}, \frac{\Delta y}{|\lambda_y|}\right) \tag{13}$$

with the added constraint that $\mathrm{CFL} \leq 1$ to maintain stability.

Contrary to classical Newtonian hydrodynamics, the recovery of primitive variables from the conserved ones requires additional numerical effort. While the conserved variables can be computed from the primitive ones via Eq. (5) easily, a direct mapping form conserved to primitive variables does not exist. Therefore, a root-finding algorithm must be deployed in their computation. eCOS follows the method given in appendix D of [9] which relies on the solution of

$$p - \bar{p}[\rho(\boldsymbol{U}, p), \epsilon(\boldsymbol{U}, p)] = 0, \tag{14}$$

where p is the pressure to be found and $\bar{p}[\rho(\boldsymbol{U}, p), \epsilon(\boldsymbol{U}, p)]$ is the pressure found via the ideal-fluid equation of state in terms of the conserved variables $\boldsymbol{U}$ and p itself. Eq. (14) is solved by means of a Newton–Raphson root-finding algorithm with a convergence criterion established by computing the L_2 error norm. In general, the root-finding algorithm converges within 11 iterations or fewer with a permitted tolerance of 10^{-8}.

The methods described herein provide an accurate and stable solution to the governing equations of RHD. Their performance is evaluated next by a series of one-dimensional and two-dimensional test cases to validate their implementation.

4. VALIDATION TEST CASES

To first understand whether numerical methods are implemented and performing correctly, a series of one-dimensional test cases must be completed. Such test cases provide an understanding of the code's ability to handle numerical discontinuities and resolve correct wave patterns. They also provide an indication of the benefits of one particular choice of numerical method other another. The one-dimensional Riemann problems have initial conditions specified by

$$\boldsymbol{\omega}(x) = \begin{cases} \boldsymbol{\omega}_L, & \text{for } x > x_{MID} \\ \boldsymbol{\omega}_R, & \text{for } x < x_{MID} \end{cases} \tag{15}$$

where $\boldsymbol{\omega}_{L,R}$ corresponds to the initial primitive variables to the left and right of the initial discontinuity in which $\boldsymbol{\omega}_{L,R} = (\rho,\, u,\, v,\, p)_{L,R}$. The midpoint of the one-dimensional domain is always $x_{MID} = 0.5$, the total simulation time is $t = 0.4s$ and for all cases the adiabatic index is $\Gamma = 5/3$.

The following tests have been performed by many authors, details of which are summarised in [1, 2]. Results are compared with the exact solution provided by the code detailed in [10] which enables direct quantitative comparison. 1D-RP-1, displayed in Fig. 1 (top), has initial conditions

$$\boldsymbol{\omega}_L = (10, 0, 0, 40/3),$$
$$\boldsymbol{\omega}_R = (1, 0, 0, 10^{-6}). \quad (16)$$

This test depicts a mildly relativistic blast wave with a left-going rarefaction wave, a contact discontinuity and shock-wave propagating rightward.

A highly relativistic blast wave is resolved in 1D-RP-2 which maintains the same wave pattern as the previous case. However, it is more demanding in terms of the code's capability to resolve the thin, high-density shell and correctly capture the contact discontinuity. 1D-RP-2 is displayed in Fig. 1 (middle) and has initial conditions

$$\boldsymbol{\omega}_L = (1, 0, 0, 1000),$$
$$\boldsymbol{\omega}_R = (1, 0, 0, 0.01). \quad (17)$$

Finally, the third test includes an initial tangential velocity that vastly modifies the wave structure. This physical effect is not present within Newtonian hydrodynamics because in RHD the momentum equations are coupled with one another, see [11] — this subsequently provides an extremely demanding test case that only until recently RHD codes were able to resolve. 1D-RP-3 displayed in Fig. 1 (bottom) has initial conditions

$$\boldsymbol{\omega}_L = (1, 0, 0, 1000),$$
$$\boldsymbol{\omega}_R = (1, 0, 0.99, 0.01). \quad (18)$$

In all cases good agreement with the exact solution is found. The higher-order WENO schemes provide a sharper profile than its lower-order counterparts however in certain cases e.g. 1D-RP-1, oscillations are present for the higher-order schemes that are visible in the density profile. Similarly, for 1D-RP-3 a slight over-shooting of the predicted high-density region is also observed. Errors computed using the L_2 error norm are presented in Tab. 1 for quantitative comparison.

A two-dimensional test case consisting of a relativistic double-Mach reflection is reported in Fig. 2. Initial conditions for this test follow those found in [5]. A strong shock-wave making an angle of $60°$ with respect to the x-axis is set to propagate rightward. A reflective boundary condition is imposed along the lower x-axis at $x > 1/6$. The top domain boundary is set to either pre-shock or post-shock flow conditions depending on the shock-wave position. Inflow and outflow boundary conditions are prescribed to the left and right domain boundary, respectively. Any issues with four different boundary condition implementations can then be found in one test case. An insight can be gained into the correct shock propagation speed in all directions and indicate whether the *Carbuncle problem* is present in the solution, see [12].

Fig. 1: One-dimensional Riemann problems 1D-RP-1 (top), 1D-RP-2 (middle) and 1D-RP-3 (bottom) achieved using the HLL Riemann solver varying WENO schemes.

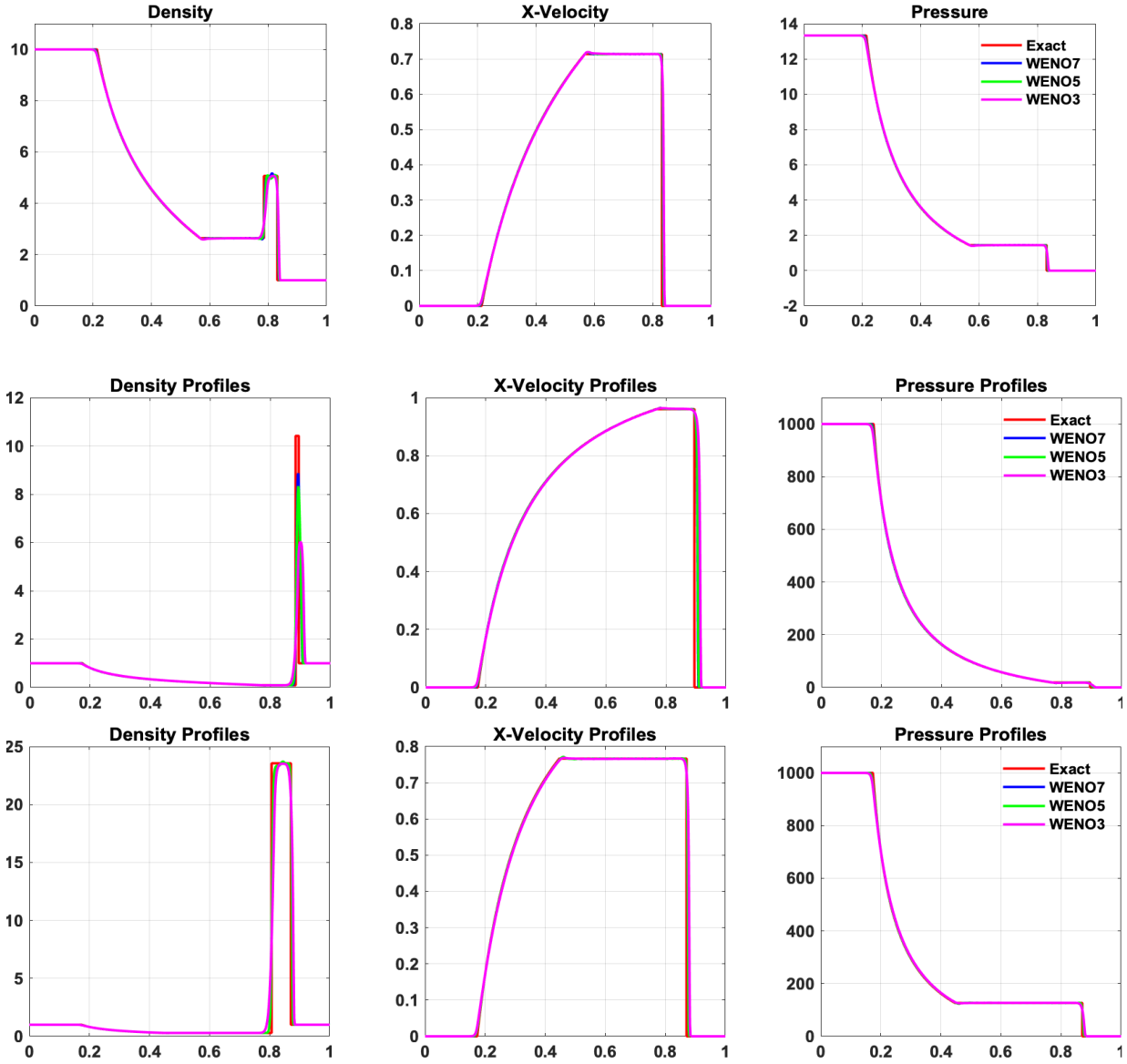

Fig 2: Two-dimensional double-Mach reflection at time t=4.0s using WENO5 spatial reconstruction and HLL Riemann solver. The mesh resolution is 1600 × 400 cells.

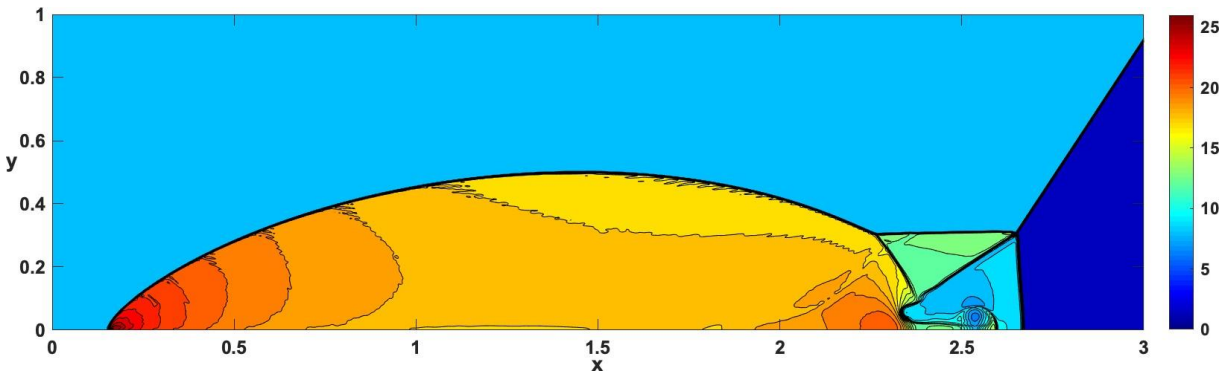

	L_2 Error Norm		
	Density	***x*-Velocity**	**Pressure**
1D-RP-1			
WENO3	5.365×10^{-2}	1.436×10^{-1}	1.458×10^{-2}
WENO5	4.769×10^{-2}	1.286×10^{-1}	1.283×10^{-2}
WENO7	4.473×10^{-2}	1.222×10^{-1}	1.119×10^{-2}
1D-RP-2			
WENO3	7.658×10^{-1}	3.175×10^{-1}	1.367×10^{-2}
WENO5	6.325×10^{-1}	2.545×10^{-1}	8.937×10^{-3}
WENO7	6.150×10^{-1}	2.473×10^{-1}	7.140×10^{-3}
1D-RP-3			
WENO3	3.511×10^{-1}	1.262×10^{-1}	2.094×10^{-2}
WENO5	2.786×10^{-1}	1.020×10^{-1}	1.562×10^{-2}
WENO7	3.511×10^{-1}	1.262×10^{-1}	1.895×10^{-2}

Table 1: Calculations of L_2 Error Norm for the one-dimensional Riemann problems using the HLL Riemann solver with varying orders of WENO spatial reconstruction.

Because different shock-waves and discontinuities are generated, where some should be straight lines with different angles with respect to the grid axis, a deviation from a straight-line shock should be looked upon with caution. If a numerical recipe has insufficient numerical dissipation, this may occur giving rise to the aforementioned Carbuncle problem. Using the HLL Riemann solver with WENO5 reconstruction we can report the absence of this unphysical phenomena. The test, along with its predeceasing one-dimensional counterparts indicates the robustness of the numerical implementation and its ability at resolving flow features under extreme conditions.

5. CONCLUSIONS

In this work the governing equations of relativistic hydrodynamics (RHD) have been discussed and presented in a form suitable for modern-day High-Resolution Shock-Capturing (HRSC) methods to be applied. The spectral decomposition of the governing equations provides real and distinct eigenvalues that permit the application of such methods. The eigenvalues enable the computation of the smallest and largest signal velocities within the system that can be used to evaluate the intercell numerical flux using the HLL approximate Riemann solver. This method, along with the other necessary numerical ingredients are discussed in the context of relativistic hydrodynamics. The application of these methods is then demonstrated via a series of demanding one- and two-dimensional test cases in which good agreement with the exact solution and current results available in the literature is found. As a result, this solver is commissioned for application to cutting-edge problems in this field such as the relativistic Richtmyer–Meshkov instability presented in Part II. of this work.

REFERENCES

[1] **J.M. Martí and E. Müller:** *Numerical Hydrodynamics in Special Relativity*, Living Reviews in Relativity, 2003., DOI: 10.12942/lrr-2003-7

[2] **J.M. Martí and E. Müller:** *Grid-based Methods in Relativistic Hydrodynamics and Magnetohydrodynamics*, Living Reviews in Computational Astrophysics, 2015., DOI: 10.1007/lrca-2015-3

[3] J**. Vredevoogd and S. Pratt:** *Viscous hydrodynamics and relativistic heavy ion collisions*, Physical Review C*,* Vol. 85, No. 4, 2012., DOI: 10.1103/PhysRevC.85.044908

[4] **L.P. Csernai:** *Advances in Relativistic Fluid Dynamics, Observables, and Applications — In Memorial Walter Greiner*, EPJ Web of Conferences*,* Vol. 182, 2012., DOI: 10.1051/epjconf/201818201002

[5] **J. N.-d. l. Rosa and C.-D. Munz:** *XTROEM-FV: a new code for computational astrophysics based on very high order finite-volume methods — II. Relativistic hydro- and magnetohydrodynamics,* Monthly Notices of the Royal Astronomical Society, Vol. 460, pp. 535-559, 2016., DOI: 10.1093/mnras/stw999

[6] **J.M. Martí, J.M. Ibáñez and A. Miralles:** *Numerical relativistic hydrodynamics: a local characteristic approach,* Physical Review D*,* Vol. 43, No. 12, pp. 3794-3801, 1991.

[7] **A. Anile:** *Relativistic Fluids and Magneto-Fluids: With Applications in Astrophysics and Plasma Physics*, Cambridge University Press, 1989.

[8] **A. Harten:** *Laws, High Resolution Schemes for Hyperbolic Conservation*, International Journal for Numerical Methods in Fluids*,* Vol. 49, pp. 357-393, 1983.

[9] **L. Rezzolla and O. Zanotti:** *Relativistic Hydrodynamics*, Oxford University Press, 2013.

[10] **B. Giacomazzo and L. Rezzolla:** *The exact solution of the Riemann problem in relativistic magnetohydrodynamics*, Journal of Fluid Mechanics*,* Vol. 562, pp. 223-259, 2006., DOI: 10.1017/S0022112006001145

[11] **J.A. Pons, J.M. Martí and E. Müller:** *The exact solution of the Riemann problem with non-zero tangential velocities in relativistic hydrodynamics*, Journal of Fluid Mechanics*,* Vol. 422, pp. 125-139, 2000., DOI: 10.1017/S0022112000001439

[12] **J. Quirk:** *A contribution to the great Riemann solver debate*, NASA Langley Research Center, Hampton, Virginia, 1992., DOI: 10.1002/fld.1650180603

[13] **G. A. Mignone:** *An HLLC Riemann solver for relativistic flows - I. Hydrodynamics*, Monthly Notices of the Royal Astronomical Society*,* Vol. 364, pp. 126-136, 2005., DOI: 10.1111/j.1365-2966.2005.09546.x

[14] **C. Shu:** *High Order Weighted Essentially Nonoscillatory Schemes for Convection Dominated Problems*, SIAM Review*,* Vol. 51, no. 1, 2009., DOI: 10.1137/070679065

[15] **E. Toro:** *Rieman Solvers and Numerical Methods for Fluid Dynamics*, Springer-Verlag, 2009., DOI: 10.1007/b79761_5

[16] **L. Zanna and N. Bucciantini:** *An efficient shock-capturing central-type scheme for multidimensional relativistic flows I. Hydrodynamics*, Astronomy and Astrophysics*,* Vol. 390, pp. 1177-1186, 2002., DOI: 10.1051/0004-6361:20020776

[17] **A. Tchekhovskoy, J.C. McKinney and R. Narayan:** *WHAM: a WENO-based general relativistic numerical scheme — I. Hydrodynamics*, Monthly Notices of the Royal Astronomical Society*,* Vol. 379, pp. 469-497, 2007., DOI: 10.1111/j.1365-2966.2007.11876.x